Supplementary Materials for "On The Diffusion of Sticky Particles in 1-D"

Joshua DM Hellier* and Graeme J Ackland[†] SUPA, School of Physics and Astronomy, University of Edinburgh, Mayfield Road, Edinburgh EH9 3JZ, United Kingdom (Dated: March 7, 2018)

Lattice MFT Derivation. Let the ensemble-averaged occupation probability of the i^{th} site at time t be $\rho_i(t)$. In the mean-field approximation regime this is assumed to be independent of $\rho_j(t)$ for $j \neq i$ at equal times. Therefore, we can condition on the probability of the i^{th} site being occupied at a given time t simply by multiplying by $\rho_i(t)$. If the i^{th} site is full, then the rate at which it empties is the sum of the probabilities that the $(i+1)^{\text{th}}$ and $(i-1)^{\text{th}}$ sites are empty, multiplied by a rate which depends on the occupation probability of the $(i+2)^{\text{th}}$ and $(i-2)^{\text{th}}$ sites respectively. Therefore in the MFT the rate at which the i^{th} site empties is

$$\frac{1}{\tau_0} (1 - \rho_{i-1}) \left[(1 - \rho_{i+1}) + \lambda \rho_{i+1} \right]
+ \frac{1}{\tau_0} (1 - \rho_{i+1}) \left[(1 - \rho_{i-1}) + \lambda \rho_{i-1} \right].$$
(1)

Similarly, if the $(i)^{th}$ site is unoccupied, it fills with rate

$$\frac{1}{\tau_0} \left\{ \rho_{i+1} \left[\lambda \rho_{i+2} + (1 - \rho_{i+2}) \right] + \rho_{i-1} \left[\lambda \rho_{i-2} + (1 - \rho_{i-2}) \right] \right\}.$$
(2)

If we now multiply the filling and emptying rates of site i by its occupation probability and the complement respectively, we obtain the final result that

$$\tau_0 \frac{\partial \rho_i}{\partial t} = (1 - \rho_i) \left[(1 - \zeta \rho_{i-2}) \rho_{i-1} + (1 - \zeta \rho_{i+2}) \rho_{i+1} \right] - \rho_i \left[2\zeta \rho_{i-1} \rho_{i+1} - (3 - \zeta) (\rho_{i-1} + \rho_{i+1}) + 2 \right].$$
(3)

MFT Continuum Limit. To obtain the continuum limit of the MFT simply substitute $\rho_i(t) \to \rho(x,t)$, $\rho_{i+m}(t) \to \rho(x+am,t)$ into Eq. 3. Then, Taylor expand around x for small a, neglecting terms of $\mathcal{O}(a^4)$. Doing this and collecting terms we find that

$$\tau_0 \frac{\partial \rho}{\partial t} = a^2 \left[1 - \zeta \rho (4 - 3\rho) \frac{\partial^2 \rho}{\partial x^2} \right]$$

$$+ 2a^2 \zeta (3\rho - 2) \left(\frac{\partial \rho}{\partial x} \right)^2 + \mathcal{O}(a^4),$$
(4)

which can be factorized into the more familiar continuity equation

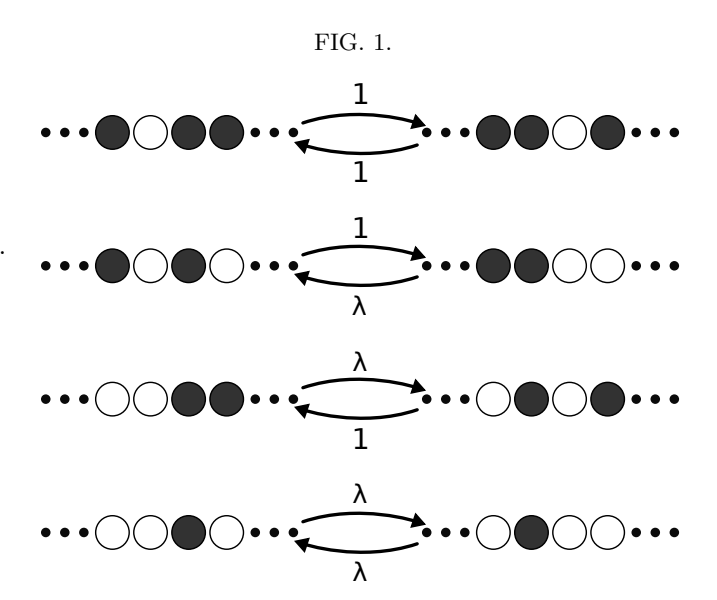
$$\frac{\partial \rho}{\partial t} = \frac{a^2}{\tau_0} \frac{\partial}{\partial x} \left\{ \left[1 - \zeta \rho \left(4 - 3\rho \right) \right] \frac{\partial \rho}{\partial x} \right\},\tag{5}$$

having dropped the higher-order terms in the continuum limit.

Steady State Solution to the Continuum MFT. Eq. 5 is simple to solve in the time-independent steady state. Integrating both sides with respect to x and using the chain rule, we see that

$$J_0(x - x_0) = \int d\rho \left[1 - \zeta \rho \left(4 - 3\rho \right) \right] = \rho + \zeta (\rho - 2) \rho^2.$$
(6)

 J_0 and x_0 may be chosen to yield the desired boundary conditions, and the equation may then be inverted by solving a cubic to find $\rho(x)$.



Detailed Balance Proof. In Fig. 1 we see all the possible transitions which may occur between local configurations. Assume that the system is now on a ring, with Llattice sites and N particles. Let us label possible system configurations by ξ and let the number of adjacencies (or "bonds") between particles is $b(\xi)$. Now for our ansatz assume that the probability of the system being in state ξ is $\lambda^{-b(\xi)}$. In the top and bottom diagrams of Fig. 1 we can see that the number of bonds on both sides is the same, as are the transition rates back and forth; thus our ansatz holds for these states, as it predicts the probabilities of the left and right configurations are the same. The middle two diagrams are the same only flipped; in the upper diagram a bond is formed going left to right and then broken going right to left, so the probability of being in the left state is λ times that of being in the right state. This is again in agreement with the detailed

balance criterion. As these are the only types of transition that may occur on a ring, we may then say that the closed system obeys detailed balance.

Additional Flow Data. Fig. 2, 3 and 4 display additional data and information from computations discussed in the main body of the Letter.

More flow plots. For the interested reader we have included for spacetime flow diagrams, show in Fig. 5. When $\lambda=0.05$, the medium consists of solid blocks surrounded by empty spaces containing a dilute gas of particles; at $\lambda=0.35$ The most interesting images (center) are those for the intermediate λ ; here we see a "lumpy" or "foamy" structure, in which small blocks of particles are being constantly created and destroyed whilst a rather minimal flow occurs across the system. The simulations did not show any hard phase transition as we vary λ ; rather, it seems that this "foamy" behavior is part of a continuous range between the extremes, containing medium-range correlations between particles. Unfortunately, computing equal-time correlation functions to the accuracy required

to draw conclusions about these correlations has proven to be extremely difficult, so we cannot find a quantitative description of the foam beyond the flow rate and density data we have discussed in this Letter. In all images in Fig. 5, long straight segments of white of black can be seen. The represent coherent motion at a characteristic velocity given by their gradient. There is nothing in the MFT to suggest what this velocity should be, and it is much smaller than the simulated system's length divided by the elapsed time, $\frac{L}{T}$, thus it must be an emergent property arising from correlated motion of self-assembled regions of high- or low-density material. However, it ha again proved difficult to analyze this numerically.

^{*} J.D.M.Hellier@sms.ed.ac.uk

[†] G.J.Ackland@ed.ac.uk

FIG. 2. Additional flow rate moments and overall system densities for the sweeps through λ with fixed boundaries.

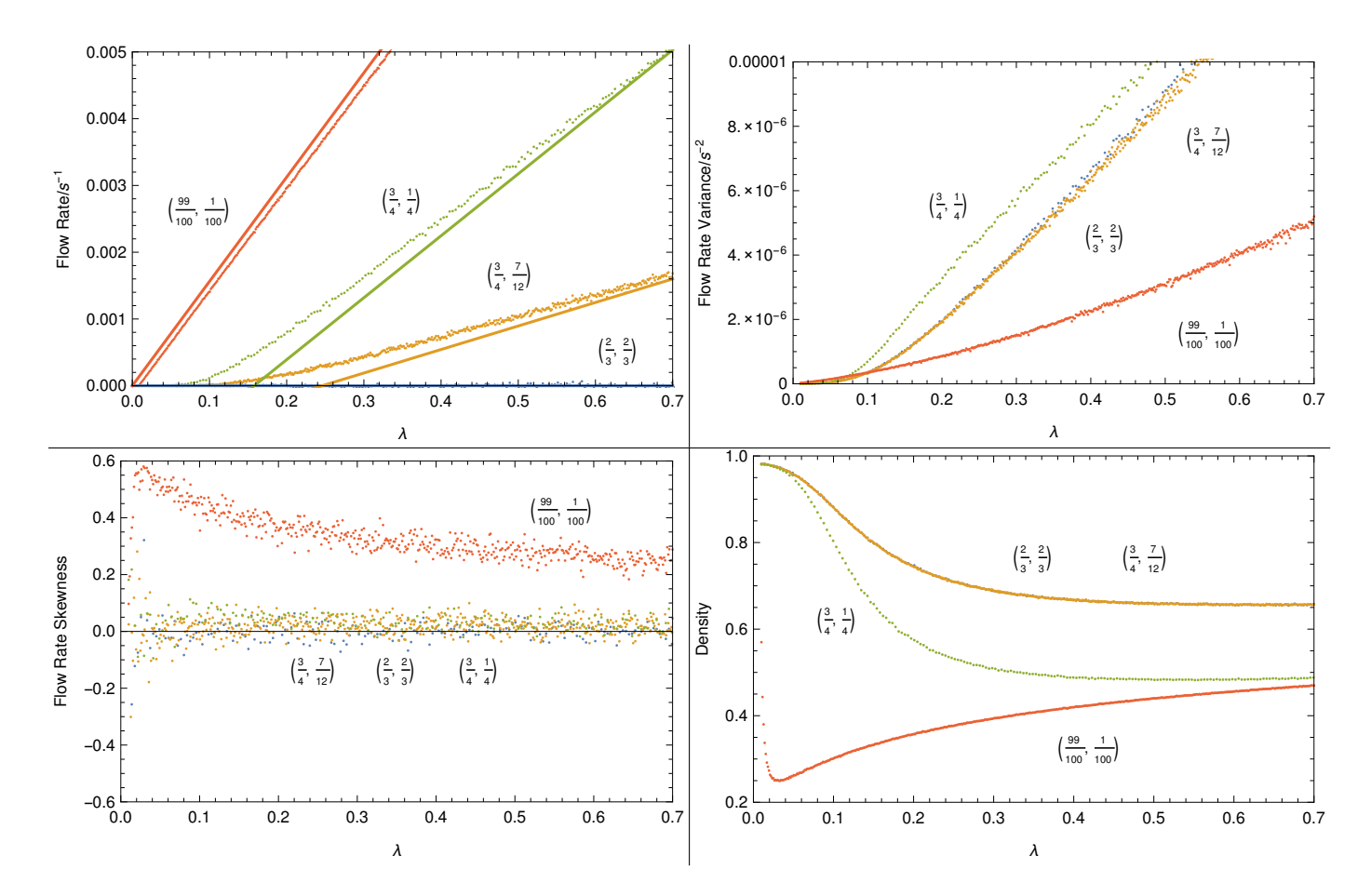


FIG. 3. Flow rate variance and average overall densities observed when varying the difference $\delta\rho$ between the boundary concentrations $(\rho_B, \rho_T) = (\rho_M + \frac{1}{2}\delta\rho, \rho_M - \frac{1}{2}\delta\rho)$ and λ . $\rho_M = \frac{1}{2}$, as in the Letter.

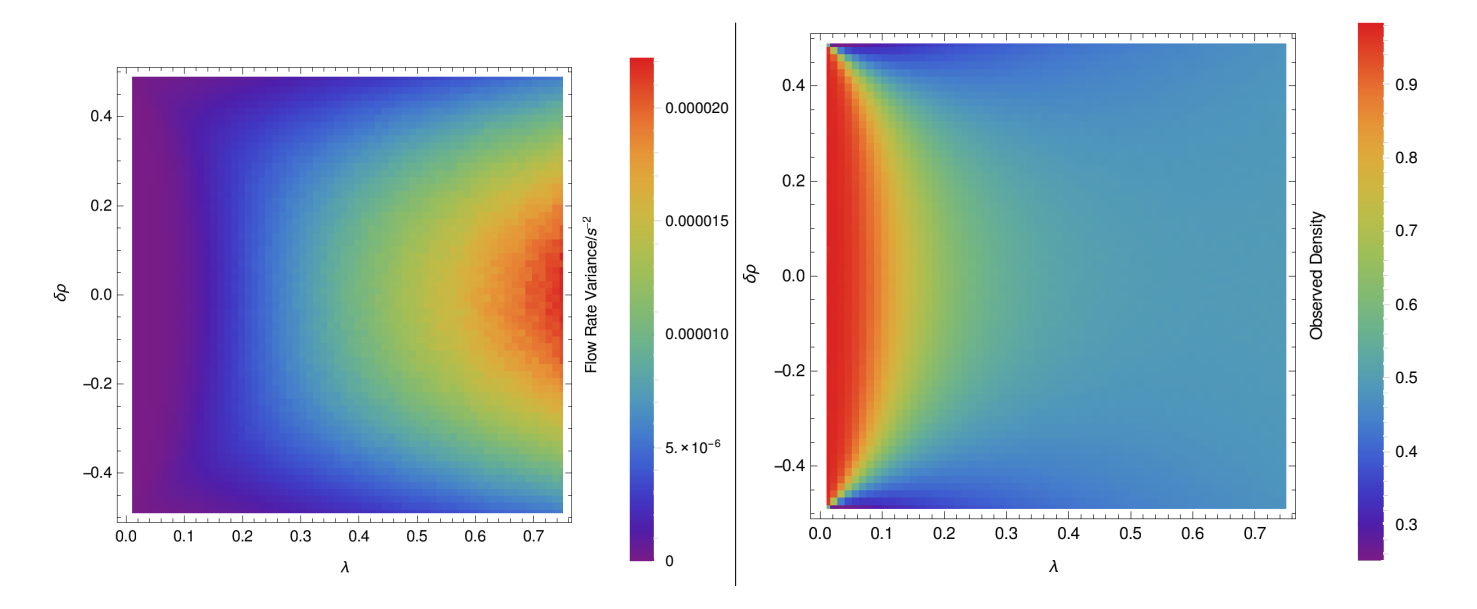


FIG. 4. These images are in addition to our computation of the effective diffusion coefficient D. The left shows the overall system density as a function of ρ_M and λ , whilst the right shows the standard error in our estimate of D. In this setup we ran the simulation for 1.6×10^8 equilibration steps, followed by 10 sets of alternating measurement and relaxation runs, of lengths 8×10^7 and 1.6×10^7 steps respectively. These results are consistent with calculations performed on smaller systems, so finite-size effects should be suppressed.

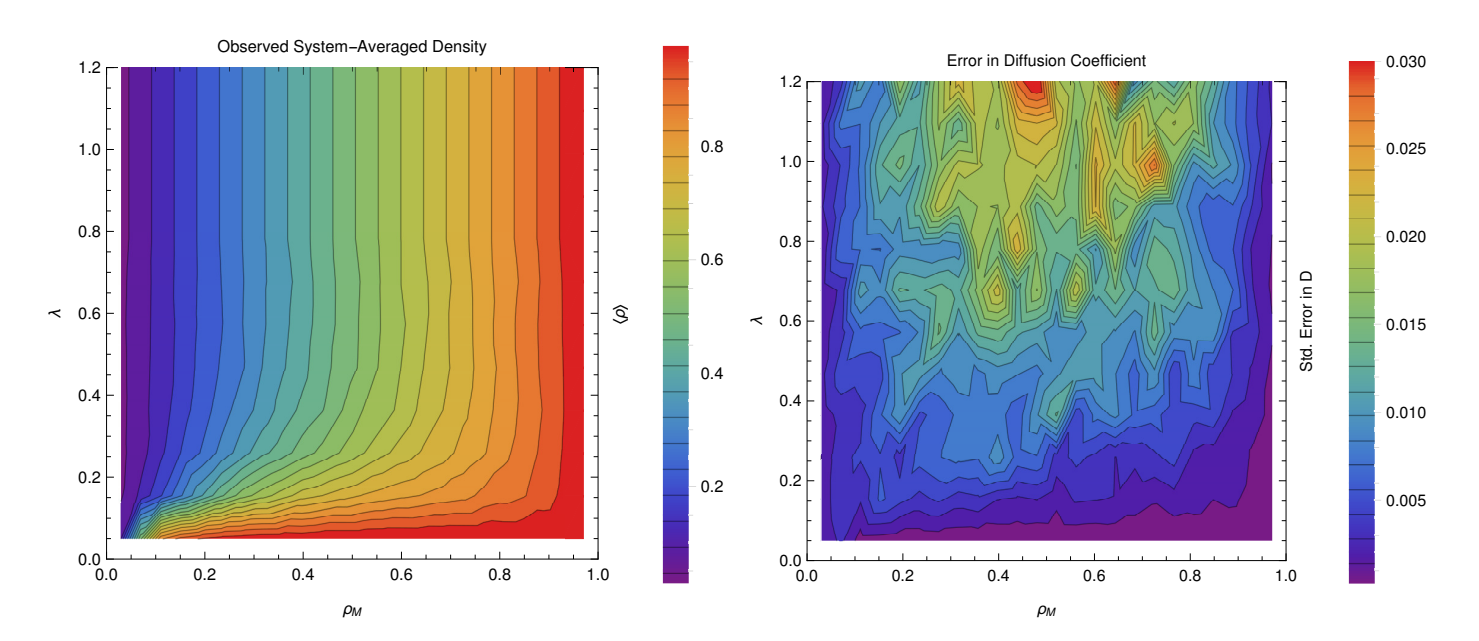


FIG. 5. The spacetime flow patterns, for λ -values of 0.05, 0.15, 0.25 and 0.35 going clockwise from top left. In each plot time runs along the x-axis, space along the y-axis, with the bottom boundary being held with a concentration of $\frac{1}{4}$ and the top at $\frac{3}{4}$. White represents full occupation, black empty, and grey shades partial occupation. The degree of occupation was calculated by taking the KMCLib record of a particular site's occupation (i.e. the Gillespie times at which the site changed occupation), assigning 0 and 1 to particles and vacancies respectively, linearly interpolating this and then integrating over times longer than a single Gillespie step but much shorter than the total time in question. In each case the total time elapsed is that taken by 2^6 Gillespie steps, and each short-time-average has been done over the total time divided by 512, the number of lattice sites; this means that on average a site would change state 8 times per pixel, although of course the real distribution is not nearly this even. Time has been rescaled this way in order to allow fair comparison of different λ -values.

